Journal of Neural Engineering

ACCEPTED MANUSCRIPT

A probabilistic recurrent neural network for decoding hind limb kinematics from multi-segment recordings of the dorsal horn neurons

To cite this article before publication: Yaser Fathi *et al* 2019 *J. Neural Eng.* in press https://doi.org/10.1088/1741-2552/ab0e51

Manuscript version: Accepted Manuscript

Accepted Manuscript is "the version of the article accepted for publication including all changes made as a result of the peer review process, and which may also include the addition to the article by IOP Publishing of a header, an article ID, a cover sheet and/or an 'Accepted Manuscript' watermark, but excluding any other editing, typesetting or other changes made by IOP Publishing and/or its licensors"

This Accepted Manuscript is **© 2018 IOP Publishing Ltd**.

During the embargo period (the 12 month period from the publication of the Version of Record of this article), the Accepted Manuscript is fully protected by copyright and cannot be reused or reposted elsewhere.
As the Version of Record of this article is going to be / has been published on a subscription basis, this Accepted Manuscript is available for reuse under a CC BY-NC-ND 3.0 licence after the 12 month embargo period.

After the embargo period, everyone is permitted to use copy and redistribute this article for non-commercial purposes only, provided that they adhere to all the terms of the licence https://creativecommons.org/licences/by-nc-nd/3.0

Although reasonable endeavours have been taken to obtain all necessary permissions from third parties to include their copyrighted content within this article, their full citation and copyright line may not be present in this Accepted Manuscript version. Before using any content from this article, please refer to the Version of Record on IOPscience once published for full citation and copyright details, as permissions will likely be required. All third party content is fully copyright protected, unless specifically stated otherwise in the figure caption in the Version of Record.

View the article online for updates and enhancements.

This content was downloaded from IP address 169.236.1.253 on 09/03/2019 at 12:01

A Probabilistic Recurrent Neural Network for Decoding Hind Limb Kinematics from Multi-Segment Recordings of the Dorsal Horn Neurons

Yaser Fathi and Abbas Erfanian

Iran Neural Technology Research Centre, Department of Biomedical Engineering, Iran University of Science and Technology (IUST), Tehran, Iran

E-mail: erfanian@iust.ac.ir

Abstract

Objective. Providing accurate and robust estimates of limb kinematics from recorded neural activities is prominent in closed-loop control of functional electrical stimulation (FES). A major issue in providing accurate decoding the limb kinematics is the decoding model. The primary goal of this study is to develop a decoding approach to model the dynamic interactions of neural systems for accurate decoding. Another critical issue is to find reliable recording sites. Up to now, neural recordings from spinal neural activities were investigated. In this paper, the neural recordings from different vertebrae in decoding limb kinematics are investigated. *Approach*. In the current study, a new generative probabilistic model with explicit considering the joint density is developed. Then, an adaptive discriminative learning algorithm is proposed for learning the model. It will be shown that the proposed generative process can be implemented by a Recurrent Neural network (RNN) with specific structure. We record the neural activities from dorsal horn neurons by using three electrodes placed in the L4, L5, and L6 vertebrae in anesthetized cats. *Main results.* Information theoretic analysis on single-joint movement and multi-segment recordings implies the rostrocaudal distribution of kinematic information. It is demonstrated that during hip movement, best decoding performance is achieved by L4 recordings. For knee and ankle movements, best decoding are achieved by L5, and L6 recordings respectively. It is also shown that the decoding accuracy using multi-segment recordings outperform decoding accuracy obtained by single-segment recording in multi-joint movement. The results also confirm the superiority of proposed probabilistic recurrent neural network (PRNN) over the conventional recurrent neural network and Kalman filter ($p < 0.05$). *Significance*. Multi-segment recordings from dorsal horn neurons as well as the proposed probabilistic recurrent network model provide a promising approach for robust and accurate decoding limb kinematics.

Keywords: probabilistic model, recurrent neural networks, decoding, dorsal root ganglia, dorsal horn.

Accepted Manuscript

1. Introduction

Decoding movement kinematics from neural signals can be utilized as the feedback information in closed-loop control of limb function through functional electrical stimulation (FES). This feedback is necessary to keep stability and respond to perturbations during a complex movement such as walking or reaching.

The feasibility of estimating kinematics information from nerve cuff recordings of muscles afferent and utilizing this information in closed-loop control of FES has been already evaluated in [1-6]. However, recordings with cuff electrodes provide information from different afferent and efferent signals and discriminating the signals arising from different nerve fibers is a challenge. Moreover, multiple nerve cuff electrode recordings are required to acquire the information from entire limb during a complex movement such as locomotion [7].

The intracortical neuronal activities [8, 9] and Electrocorticography (ECoG) signals [10-12] have been proposed as alternative sources for decoding the kinematic information. However, brain signals contain more information about the high-level locomotor states and continuous decoding of limb kinematics requires a large number of electrodes to be implanted.

Dorsal root ganglia (DRG) is also considered as an alternate source for obtaining sensory information. A wide variety of proprioceptive information converges into the central nervous system at dorsal root ganglia. The dorsal root ganglion is a collection of the cell bodies of sensory neurons that carry information from the periphery to the spinal cord. Multichannel recordings from DRG were used to decode hind limb kinematics (i.e., hip, knee, ankle joints and endpoint kinematics) [7, 13-19] and to detect sensory event [20]. However, it should be noted that the long-term chronic recordings from DRGs do not last for more than three weeks [16]. This is mostly because of the suspended structure of dorsal root ganglia, and the fact that attaching an array to it would increase the risk of tearing the roots. In contrast, the natural blood-brain barrier of the spinal cord (which the DRG and peripheral nerves lack) may provide a healthier tissue interface and prolong the quality of chronic recordings [21].

To overcome the limitation of DRG recordings, spinal cord recordings have been proposed for decoding the limb kinematics. The modulation of dorsal spinocerebellar neurons responses to the limb movement has been investigated [22-25]. The spinocerebellar system is one of the main central projections of the muscle receptors. It was reported that the activities of dorsal spinocerebellar neurons encode the global parameters of limb movement and posture rather than the specific muscle or joint parameters. Dorsal horn is an alternate location for extracting sensory information. The central branch of the sensory axon enters the dorsal horn of the spinal cord [26]. The signals recorded by a 16-channel microelectrode array implanted in the left dorsal horn of the spinal cord between the seventh and eighth cervical root, have been already used for detecting the sensory events generated by electrical stimulation in rat [21]. Eight channel dorsal horn recording was also applied to decode intravesical pressure in rat [27]. Recently, decoding the

Accepted Manuscript

hind limb kinematics using single electrode recording from the dorsal horn cells in one segment of the spinal cord has been investigated in [28].

A critical issue in decoding kinematic information from neural signals is the decoding model. Methods for decoding limb positions from the populations of sensory neurons are needed to provide accurate feedback signals during a wide range of movement conditions for closed-loop control of functional electrical stimulation [7, 13]. In early studies [14-16], linear regression methods were used to predict the hind limb kinematics (i.e. foot position, hip, knee, ankle angles) from populations of neurons in DRG [14-16]. To improve the performance of decoding the limb kinematics using neural recordings, nonlinear methods have also been employed in [17-19, 29]. In [17], particle filtering was used for decoding the hind limb kinematics using DRG recordings. However, particle filter is computationally inappropriate for real-time applications [7, 30]. In [18], it was demonstrated that fuzzy neural network (FNN) model provided more accurate estimates of limb state and generalized better than multiple linear regression methods. However, the FNN is a static neural network, in which there is no feedback, and the outputs are calculated directly based on their connection with feed-forward inputs. The static structure of the decoding method is not an efficient method for representation the nonlinear dynamic relationships between the neural signals and the limb states. Recently, a recurrent neural network (RNN) was used as a nonlinear and dynamic model to decode the ankle and knee angles from DRG 16-channel recordings [19] and demonstrated that the nonlinear model provided better decoding accuracy than multiple linear regression and Kalman filter estimators. The architecture of the RNN used in [19] takes the form of an input-output recurrent model. In this model, the delayed values of the network output were used as the input of the network for modeling the dynamics [31].

In this paper, a new method which is based on a generative model with adaptive discriminative learning algorithm is proposed for decoding hind limb kinematics from the dorsal horn neurons of the spinal cord during hind limb passive movement. In the usual approach of the generative learning, first, the joint distribution $p(y, x)$ is learned and then subsequently the output variable is predicted using the Bayes rules [32, 33]. In [34], an RNN was used as a black-box generative model and it was interpreted that the RNN can be considered as a recursive Bayesian estimation. The RNN was discriminatively trained by optimizing the log-likelihood function of the true state and it directly computed the probability of an output given an input. In [35], Kalman filter was used as a generative model with the discriminative learning for a visual state estimation task without having to explicitly create a generative model. Moreover, a linear dynamic model was considered for modeling the generating process (i.e., KF) which may not be suitable for nonlinear systems.

In the current study, a new generative probabilistic model with explicit considering the joint density is developed. Then, an adaptive discriminative learning algorithm is used for learning the generative model.

Accepted Manuscript

It will be shown that the proposed generative process can be implemented by an RNN with specific structure which is different from the conventional RNN and its structure is automatically determined by the model itself.

In previous work, the feasibility of decoding the hind limb kinematics using single electrode recording from the dorsal horn cells in one segment of the spinal cord has been investigated [28]. Due to the fact that sensory afferents of hind limb muscles are terminated rostrocaudally at different segments of spinal cord [36, 37], this study is also undertaken to examine whether the recordings from dorsal horn of multiple segments can provide more information about the limb kinematics than that from single-segment recordings.

2. Method

2.1. Probabilistic decoding model

Decoding neural signal to predict the limb positions can be considered as a regression problem. Regression analysis is a statistical technique for determining the relationship between a single dependent variable (e.g., *y*) and one or more independent variables (e.g., **X)**. To be specific, consider a general nonlinear regression model defined by

$$y_n = f(\mathbf{X}_{\boldsymbol{n}}) + \varepsilon \tag{1}$$

where $\mathbf{X}_n = [\mathbf{x}_1, \dots, \mathbf{x}_n]$, $\mathbf{x}_n$ is the feature vector at time n (i.e., firing rates of multi-unit activities of different vertebral segments and their time delayed values of order 10) and ε is an additive white-noise term of zero mean and variance σ^2. It can be shown that the optimal solution for unknown function $f(\mathbf{x})$ is equal to the conditional mean of the observable y given the regressor $\mathbf{X}$, as shown by

$$\begin{aligned} \hat{y}_n = f(\mathbf{X}_{\boldsymbol{n}}) &= E(y_n|\mathbf{X}_n) \\ &= \int y_n p(y_n|\mathbf{X}_n)\, dy_n \end{aligned} \tag{2}$$

where $p(y_n|\mathbf{X}_n)$ is the conditional probability density function (pdf) of the random variable y_n given the $\mathbf{X}_{\boldsymbol{n}}$. It can be shown that (2) can be written as (see Appendix A)

$$\hat{y}_n = \frac{\int y_n\, p(\mathbf{x}_n|y_n) \int p(y_n|y_{n-1}) p(y_{n-1}|\mathbf{X}_{n-1})\, dy_{n-1} dy_n}{\int p(\mathbf{x}_n|y_n) \int p(y_n|y_{n-1}) p(y_{n-1}|\mathbf{X}_{n-1})\, dy_{n-1}\ dy_n} \tag{3}$$

The denominator of (3) works as a normalization factor and can move under the integral of the numerator. Estimating the integrals with Riemann sum, we have

$$\hat{y}_n = \sum_{k=1}^{K} y_n^k a_n^k \tag{4}$$

$$a_n^k = \frac{p\left(\mathbf{x}_n \middle| y_n^k\right) \sum_{k_1=1}^{K} P\left(y_n^k \middle| y_{n-1}^{k_1}\right) P\left(y_{n-1}^{k_1} \middle| \mathbf{X}_{n-1}\right)}{\sum_{k_2=1}^{K} p\left(\mathbf{x}_n \middle| y_n^{k_2}\right) \sum_{k_1=1}^{K} P\left(y_n^{k_2} \middle| y_{n-1}^{k_1}\right) P\left(y_{n-1}^{k_1} \middle| \mathbf{X}_{n-1}\right)} \tag{5}$$

Here, K can be considered as the number of the hidden states and y_n^k is the hidden state at time n. The system state at time n is a weighted sum of hidden states (4). According to hidden Markov model,

Accepted Manuscript

$P(y_n^k|y_{n-1}^{k_1})$ can be interpreted as the probability of transition from state k_1 at time $n-1$ to state k at time *n*, known as the transition probability, and $p(\mathbf{x}_n|y_n^k)$ is the probability density function of observing neural signal *x* given the state k at time *n*, known as the likelihood or emission density function.

2.2. Probabilistic recurrent neural network (PRNN)

To estimate y_n, both a_n^k and y_n^k should be estimated. To estimate the posterior probability of the system state given the input data (i.e., a_n^k), we have to estimate the likelihood and transition probabilities. The likelihood density function is approximated with a Gaussian mixture model (GMM). In the GMM, an unknown distribution can be approximated by a weighted sum of a finite number of components with Gaussian densities [38] as follows:

$$p(\mathbf{x}_n|y_n^k) = \sum_{m=1}^{M} r^{k,m} g(\mathbf{x}_n; k, m) \tag{6}$$

where, *M* is the total component of the mixture, $r^{k,m}$ is the mixture coefficient for each component $\{k, m\}$, and $g(\mathbf{x}_n; k, m)$ is a Gaussian distribution defined as follows:

$$g(\mathbf{x}_n; k, m) = (2\pi)^{-\frac{D}{2}} |\mathbf{\Sigma}^{k,m}|^{-\frac{1}{2}} \exp[\psi_n^{k,m}] \tag{7}$$

$$\psi_n^{k,m} = -\frac{1}{2}(\mathbf{x}_n - \mu^{k,m})^T (\mathbf{\Sigma}^{k,m})^{-1} (\mathbf{x}_n - \mu^{k,m}) \tag{8}$$

where $\mathbf{\Sigma}^{k,m}$ is covariance matrix that could be learned from the input data. Substituting (6) into (5), we get

$$a_n^k = \frac{\tilde{a}_n^k}{\sum_{k_2}^{K} \tilde{a}_n^{k_2}} = \frac{\sum_{k_1=1}^{K} \sum_{m=1}^{M} r^{k,m} \gamma^{k_1,k} g(\mathbf{x}_n; k, m) a_{n-1}^{k_1}}{\sum_{k_2=1}^{K} \sum_{k_1=1}^{K} \sum_{m=1}^{M} r^{k_2,m} \gamma^{k_1,k_2} g(\mathbf{x}_n; k_2, m) a_{n-1}^{k_1}} \tag{9}$$

where $\gamma^{k_1,k} = P(y_n^k|y_{n-1}^{k_1})$. The model (5) can be incorporated into a three-layer recurrent neural network as shown in figure 1. Let

$$\xi_n^{k_1,k,m} = r^{k,m} \gamma^{k_1,k} g(\mathbf{x}_n; k, m) \tag{10}$$

We linearize (10) by taking its logarithm as follows:

$$log\ \xi_n^{k_1,k,m} \triangleq \mathbf{w}^{k_1,k,m^T} \tilde{\mathbf{x}}_n \tag{11}$$

where $\mathbf{w}$ and $\tilde{\mathbf{x}}$ are defined as

$$\tilde{\mathbf{x}}_n = [1, \mathbf{x}_n{}^T, (x_n^1)^2, x_n^1 x_n^2, \dots, x_n^1 x_n^D, (x_n^2)^2, x_n^2 x_n^3, \dots, x_n^2 x_n^D, \dots, (x_n^D)^2]^{\mathrm{T}} \tag{12}$$

$$\mathbf{w}^{k_1,k,m} = [w_0^{k_1,k,m}, \sum_{j=1}^{D} s_{j1}^{k,m} \mu_j^{k,m}, \dots, \sum_{j=1}^{D} s_{jD}^{k,m} \mu_j^{k,m}, -\frac{1}{2} s_{11}^{k,m},$$

$$-s_{12}^{k,m}, \dots, -\frac{1}{2}(2 - \delta_{jl}) s_{jl}^{k,m}, \dots, -\frac{1}{2} s_{DD}^{k,m}] \tag{13}$$

$$w_0^{k_1,k,m} = log\ \gamma^{k_1,k} + log\ r^{k,m} - \frac{D}{2} log\ 2\pi - \frac{1}{2} log|\mathbf{\Sigma}^{k,m}|$$

$$-\frac{1}{2} \sum_{j=1}^{D} \sum_{l=1}^{D} s_{jl}^{k,m} \mu_j^{k,m} \mu_l^{k,m} \tag{14}$$

where $s_{jl}^{k,m}$ are the elements of the inverse covariance matrix $(\mathbf{\Sigma}^{k,m})^{-1}$. δ_{jl} is 1 if *j*=*l* and otherwise 0.

Accepted Manuscript

The overall process is incorporated into a recurrent neural network demonstrated in figure 1. The input vector $\mathbf{x}$ ($\mathbf{x}\epsilon\Re^{D}$) is converted into the vector $\tilde{\mathbf{x}}$ ($\tilde{\mathbf{x}}\epsilon\Re^{\tilde{D}}$), according to nonlinear transformation (12), in which constitutes the input of the RNN. In the first layer, each unit receives the input from the input layer weighted by the coefficient $w_{\tilde{d}}^{k_1,k,m}$ and outputs the *a posteriori* probability of each component, $\xi_n^{k_1,k,m}$. Each unit in the second layer outputs multiplication of the transition probability by the emission density function for each component. The outputs from the second layer weighted by the coefficient a_{n-1}^{k} are added up and input into the third layer. At last, the outputs from the third layer weighted by the coefficient $y_n^k/\mathcal{N}$ is added up and generate the prediction of the target. The $\mathcal{N}$ is generated by adding up the output of the units in the third layer.

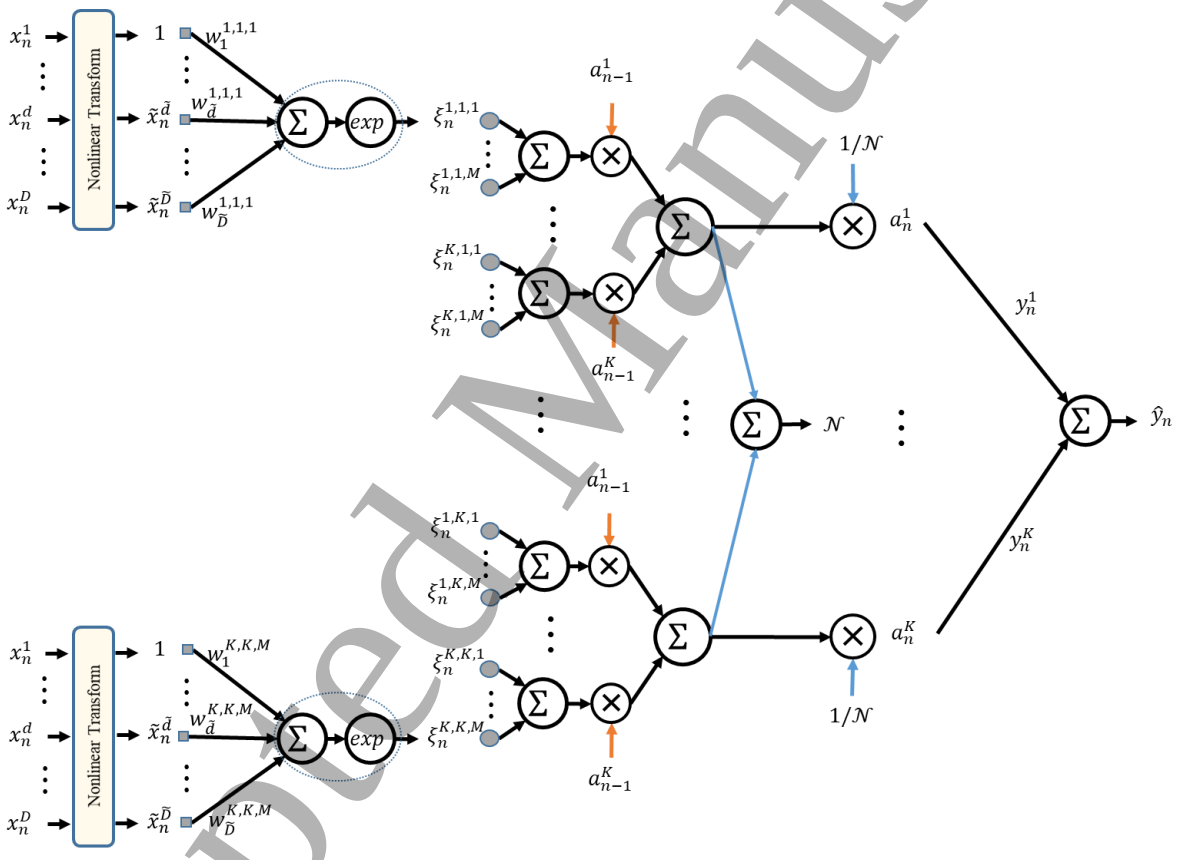

Figure 1. Structure of proposed probabilistic recurrent neural network (PRNN). The network contains three main layers. The weights in the input layer, $w_{\tilde{d}}^{k_1,k,m}$, correspond to probabilistic parameters of the model. The weights in the output layer, y_n^k, correspond to hidden states of the model (possible outputs). a_{n-1}^{k} is the feedback connection from the hidden layer (second layer) to itself.

The parameters of the recurrent network structure are $\mathbf{w}$ and y_n^k and Levenberg-Marquardt (LM) adaptation rule is employed to train the proposed recurrent network [39, 40]. To reduce the computational complexities, we consider a diagonal covariance matrix rather than a full covariance matrix. In this case, the parameters $\mathbf{w}$ and $\tilde{\mathbf{x}}$ are defined as follows:

$$\tilde{\mathbf{x}}_n = [1, \mathbf{x}_n{}^T, (x_n^1)^2, (x_n^2)^2, \ldots, (x_n^D)^2]^{\mathrm{T}} \quad (15)$$

Accepted Manuscript

$$\mathbf{w}^{k_1,k,m} = [w_0^{k_1,k,m}, \mu_1^{k,m} s_{11}^{k,m}, \dots, \mu_D^{k,m} s_{DD}^{k,m}, -\frac{1}{2} s_{11}^{k,m}, \dots, -\frac{1}{2} s_{dd}^{k,m}, \dots, -\frac{1}{2} s_{DD}^{k,m}] \quad (16)$$

$$w_0^{k_1,k,m} = log\, \gamma^{k_1,k} + log\, r^{k,m} - \frac{D}{2} log\, 2\pi - \frac{1}{2} log|\mathbf{\Sigma}^{k,m}| - \frac{1}{2} \sum_{j=1}^{D} s_{jj}^{k,m} (\mu_j^{k,m})^2 \quad (17)$$

For diagonal covariance matrix, the dimension of the $\tilde{\mathbf{x}}_n$ is $\tilde{D}_{diag} = 1 + 2D$, while it is $\tilde{D}_{full} = 1 + \frac{D(D+3)}{2}$ for full covariance matrix. Hence, the number of parameters that should be learned is significantly decreased and the computational complexities are reduced.

3. Simulation study

3.1 Generating synthetic data

To provide an insight into the capability of PRNN, we performed simulation analysis on synthetic data. The process of generating synthetic data used in this section is similar to [41, 42]. In summary, two-dimensional movement of the hand was considered to be $p_x(n) = 3cos(\pi n/3)$, $p_y(n) = 2sin(\pi n/2)$, where $p_x(n)$ and $p_y(n)$ are hand position in *x* and *y* directions, respectively. The derivative of hand position in two dimensions is defined by the vector, $\mathbf{v}(n)$, indicating the velocity of hand movement. The tuning function that specifies the average of firing rate for each neuron, is defined as $\lambda_i(\mathbf{v}(n)) = \max(b_i + s_i \mathbf{v}(n).\mathbf{r}_i, 0)$. The term $\mathbf{r}_i$ indicates the preferred direction of the i_{th} neuron, b_i and s_i are the base firing rate and directional sensitivity, respectively. Parameters for each neuron are chosen randomly. Finally, the firing rate of each neuron (f_i) was obtained based on Poisson distribution as follows:

$$p(f_i(n)|\mathbf{v}(n)) \sim Poisson(\lambda_i(\mathbf{v}(n)))$$

3.2 Simulation results

The simulation was performed with 10 neurons. The firing rate was generated for a period of 20 s. The firing rates were sampled with different sampling rates including 2.5 Hz, 5 Hz, 10 Hz, 20 Hz, and 40 Hz to evaluate the performance of the different decoding models. We used three-fold cross-validation for training and testing the decoding models. Half of the data were assigned for training the model (50%), 17% for validation, and the remaining 33% of the data for testing. The parameters *K* in (4) and *M* in (6) were empirically set to values $K = 3$ and $M = 2$ to achieve the best decoding performance.

Figures 2(a)-(d) show the average of decoding performance using the proposed PRNN model, Kalman filter [43], and conventional recurrent neural network which is based on the state-space model [31]. In this architecture, the output of the hidden layer is fed back to the input layer via a bank of unit-time delays. The hidden layer of the RNN used in this simulation consists of five neurons. The results show that Kalman filter reaches faster to its asymptotic error but it has a greater asymptotic error than other two approaches [32]. This might be due to the misspecification problem of the generative models [33]. The RNN performs well when enough number of training samples are available (high sampling rate), but its performance deteriorates for a small number of training samples (low sampling rate). The results show that the proposed

Accepted Manuscript

model (PRNN) outperforms both Kalman filter and RNN for any sampling rate. PRNN benefits discriminative learning, which avoids misspecification, especially for high sampling rate. For a small number of training samples, it prevents overfitting by putting bounds on the network structure. An example of decoding for each method is also shown in figures 2(e)-(g).

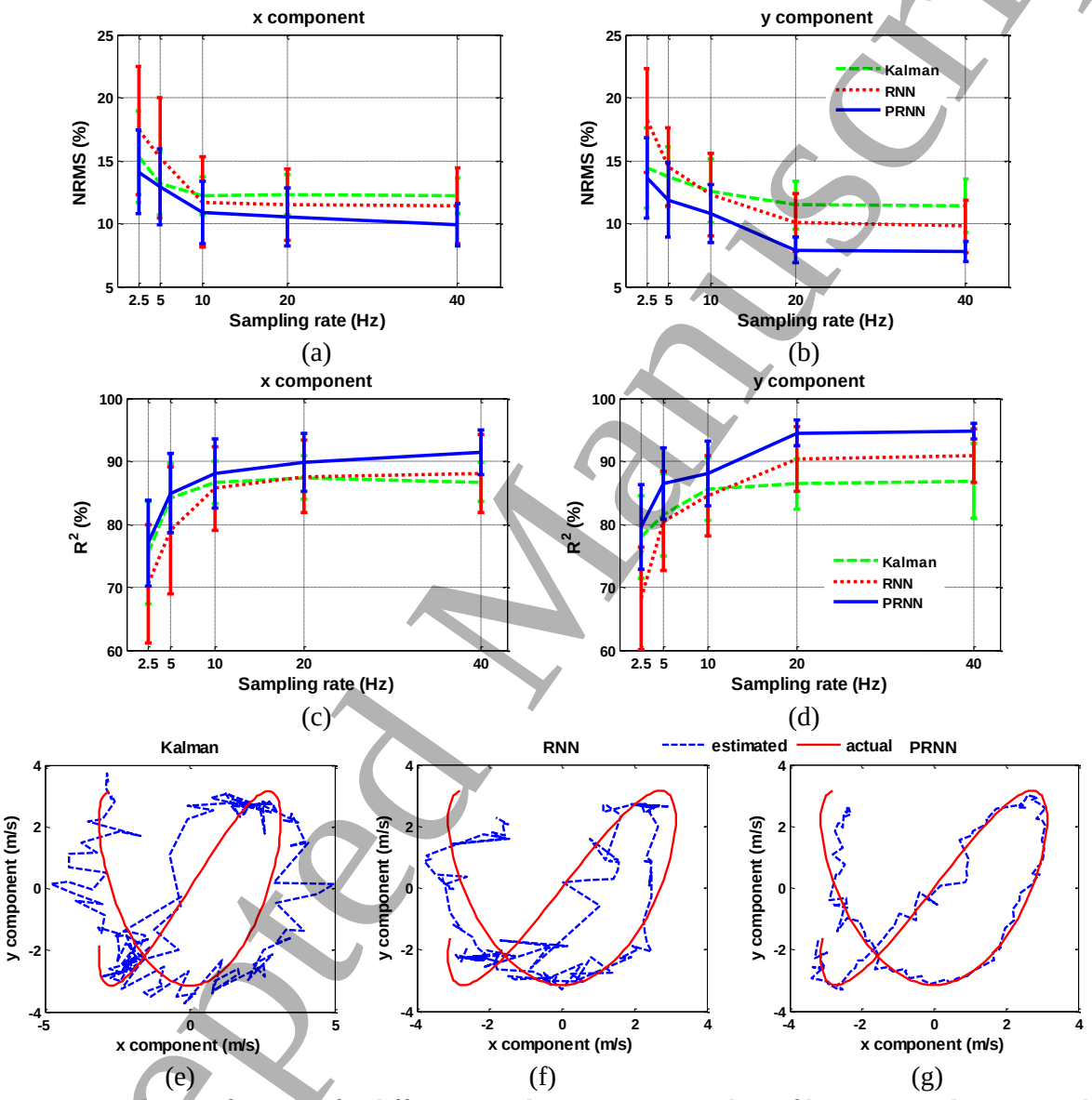

Figure 2. Decoding performance for different sampling rates using Kalman filter, RNN and PRNN methods in x-direction (a), (c) and y-direction (b), (d). Examples of decoded velocity trajectories using Kalman (e), RNN (f), and PRNN (g).

Accepted Manuscript

4. Experimental procedure

The experiments were conducted in the Neural Engineering laboratory at Iran University of Science and Technology. All surgical procedures and experimental protocols involving animal models described in this paper were approved by the Animal Care and Ethics Committee of Iran Neural Technology Research Centre, Iran University of Science and Technology. The experimental protocol was performed in accordance with the recommendations for the care and use of laboratory animals. Two sets of experiments were performed. In the first set, only one joint was flexed or extended passively while other two joints were held fixed as much as possible (see supplementary video). The aim of the single-joint experiments was specifically to highlight the rostrocaudal distribution of kinematic information along the spinal segments. During each session of experiment, 10 1-min trials of experiment were conducted for each joint angle. The second set of experiments consisted of simultaneously passive movement of three joints. Each trial of the multi-joint movement lasted 10 minutes.

4.1. Animal preparation and surgical procedure

Experiments were conducted on eight adult cats (2.8-3.5 kg). Initial anesthesia was induced with intramuscular injection of ketamine (20 mg/kg) into the cranial thigh muscle. Then, the animals were maintained at a surgical level of anesthesia under isoflurane inhalation (1.0%–3.0% in O2). A partial laminectomy was performed over L4-L6 vertebrae to expose multiple spinal segments (L3-S1). It should be noted that L3-L4 spinal segments correspond to the spinal region under L4 vertebra, L5-L6 spinal segments correspond to L5 vertebral segment, and L7-S1spinal segments to L6 vertebra [44]. After laminectomy, an incision was made in the dura mater at the midline with iridectomy scissors. The animals were then mounted in a modified stereotaxic (SN-1N, NARISHIGE Group Product) setup which allows the hind limbs to hang freely in space and the spinal vertebrae L3 and L7 were clamped tightly to the frame (figure 3).

4.2 . Joint angle measurements

The hind limb kinematics were captured by the high-speed (250 fps at 1 megapixel resolution) motion capture system (Vicon Motion Systems Ltd., UK) at 100 fps with 3 cameras placed perpendicular to the sagittal plane on the right at a distance of approximately 2 m from the animal. The reflective markers were attached to the iliac crest, greater trochanter (hip joint), lateral condyle of the femur (knee joint), lateral malleolus (ankle joint), and the distal end of the fifth metatarsophalangeal (MTP) joint of the cats. Motion capture software (Tracker 2.2, Vicon, UK) was used to acquire the coordinates of the markers. Using five marker positions, three joint angles (ankle, knee, hip) were calculated using a custom Matlab program. Motion data were then downsampled to 10 Hz.

Accepted Manuscript

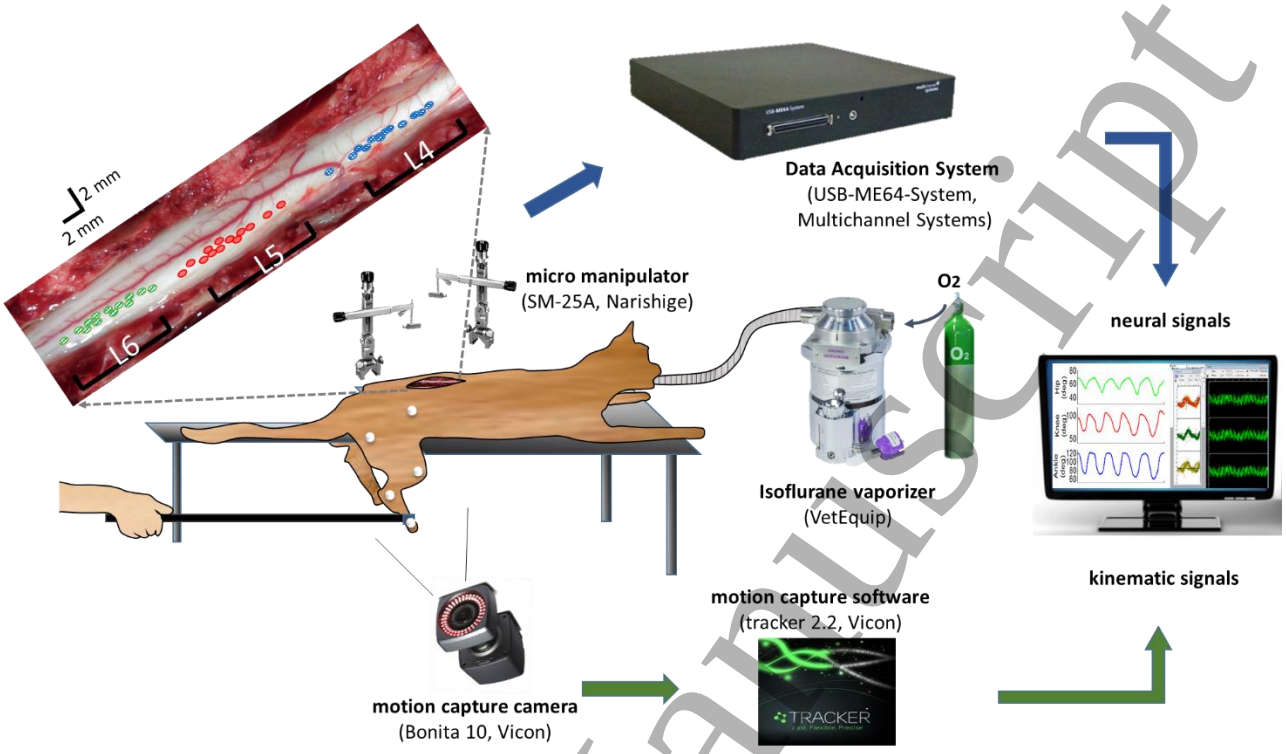

Figure 3. Experimental setup for recording neural and kinematic signals during passive movement in anesthetized cat and dorsal view of the surface of hind limb spinal cord in a representative cat. Electrode positions relative to spinal vertebra over all sessions are shown by small circles.

4.3 Neural signal recording and preprocessing

Three single-wire stainless steel electrodes with Epoxylite-insulated with 10^{o}-5^{o} tapered tip of 120 μm exposed length, 75 μm shank diameter, and 300-500 $k\Omega$ resistance (FHC Inc., Bowdoin, ME USA) were positioned in the right dorsal horn of spinal cord at L4, L5, and L6 vertebrae. Electrodes were mounted on a micromanipulator (SM-25A, NARISHIGE Group Product) which enables three-dimensional controlling and positioning of the electrodes with the minimum graduation of 10 μm. The electrode placed in the L4 vertebra, approximately 1.0-1.7 mm lateral from the midline and 1.0-1.4 mm in depth from the dorsal surface, in the L5 vertebra approximately 1.1-2.1 mm lateral from the midline and 1.2-1.8 mm deep in the L6 vertebra, approximately 1.0-1.8 mm lateral from the midline and 0.9-1.6 mm deep. To determine the best electrode position within a segment in the dorsal horn, during each session of experiment, the electrode was vertically advanced through the spinal cord dorsoventrally. Then, the electrode was removed and reinserted in 100 μm increments in three-dimensional rostrocaudally and/or mediolaterally to an adjacent location. For each position, the neural signals were recorded, graphed, and visualized online using MC_Rack software (Multichannel Systems Reutlingen, Germany) while the limb was passively moved and the correlation of neural activity with the passive movement of the limb was visually inspected. The positions that produced relatively highest correlation were selected.

Accepted Manuscript

Neural signals were amplified (programmable gain, 1000×) and recorded at 20 kHz sampling rate using a data acquisition system (USB-ME64 system, Multichannel Systems Reutlingen, Germany). The recorded raw signals were band-pass filtered between 300 and 3000 Hz. The threshold for spike detection was set to 3.5 times the estimated standard deviation of the noise of filtered signal. Spike trains of the multi-unit activities were converted to firing rates (FRs) in 100 ms bins using a sliding Gaussian window of length 250 ms overlapped by 150 ms. The resulting dataset consisted of 8 10-minute recordings (data files) from 5 cats (cat 1 - cat 5) for multi-joint movement and 70 1-min trials for each joint in the single-joint movement from three cats (cat 6 – cat 8) (Table 1). Note that during each session of experiment, the electrodes were implanted according to electrode implantation procedure and removed at the end of experiment.

Table 1. Summary of data collected from each cat.

Protocol	Cat 1	Cat 2	Cat 3	Cat 4	Cat 5	Cat 6	Cat 7	Cat 8
Multi-joint	✓	✓	✓	✓	✓	-	-	-
Single-joint	-	-	-	-	-	✓	✓	✓
Number of sessions	1	2	2	1	2	3	2	2
Number of trials per session	1	1	1	1	1	30	30	30
Trial duration (min)	10	10	10	10	10	1	1	1

5. Results

To assess the performance of the proposed method in decoding the kinematic information of the limb, the normalized root-mean-square (NRMS) of the estimation error and the coefficient of determination, R^2 value, were used. The NRMS and R^2 were defined as

$$\text{NRMS}\ (\%) = \left(\frac{\sqrt{\frac{1}{N}\sum_{n=1}^{N}(y_n-\hat{y}_n)^2}}{max(\mathbf{y})-min(\mathbf{y})}\right)\times 100 \tag{18}$$

$$R^2(\%) = \left(1-\frac{\sum_{n=1}^{N}(y_n-\hat{y}_n)^2}{\sum_{n=1}^{N}(y_n-\bar{y})^2}\right)\times 100 \tag{19}$$

where y is the measured joint angle and $\bar{y}$ is its mean value, $\hat{y}$ is the estimated angle, and N is the number of data points. Moreover, in order to evaluate the information content of the neural signals recorded from different vertebral segments, the mutual information (MI) was calculated between firing rate of each vertebral segment and hind limb kinematics. Mutual information was calculated based on an adaptive partitioning of the observation space [45]. We used three-fold cross-validation for training and testing the

Accepted Manuscript

model. Training, validation, and test were performed on each data file obtained during each trial of experiment. One round of cross-validation involves partitioning the data into three subsets performing the training on one subset with 50% of data, validating on the next subset with 17% of data, and testing on the remaining 33% of the data. The two other rounds of cross-validation were performed using different partitions with the same data size used in the first round. Then, the average of decoding performance over the 3-fold cross-validation and all trials of experiment were reported.

The parameters K in (4) and M in (6) were chosen empirically ($K = 3, M = 2$) to achieve the best decoding performance during one trial of experiment and set for all experiment trials. M indicates number of mixture component in likelihood distribution (6) and K number of hidden states (4).

Figure 4 shows the typical recorded joint angles, recorded raw neural signals and their band-pass filtered (0.3-3 kHz) signals, unsorted spike trains, and multi-unit spike waveforms during passive movement of the limb. It can be seen that the filtered neural signals (as well as the spike trains) are highly correlated with the limb movement. The limb movements as stimuli, give rise to a correlated activity in the spinal cord gray matter neurons. This suggests that reverse regression can be used to decode the limb kinematics from spinal neural signals.

5.1 Single-joint decoding

Figure 5 shows examples of the recorded joint angles and the firing rates of the multi-unit activities recorded from each segment during passive movement of each joint. In this experimental setup, only one joint is moved while two other joints were kept fixed as much as possible. It should be noted that although two joints were fixed, however, during movement of the free-joint, the fixed joints may have a little movement. It can be seen that during passive movement of the hip joint, only the firing rate recorded from the L4 vertebral segment closely follows the hip joint angle (figure 5(a)). The knee joint movements give rise to a correlated neuronal activity recorded from the L5 vertebra (figure 5(b)) and the ankle movement to the firing activity from the L6 (figure 5(c)). It can be seen that during passive movement of the knee joint, the recorded signal from L4 shows a rhythmic activity. This may be due to the movement of the hip joint during passive movement of the knee.

Accepted Manuscript

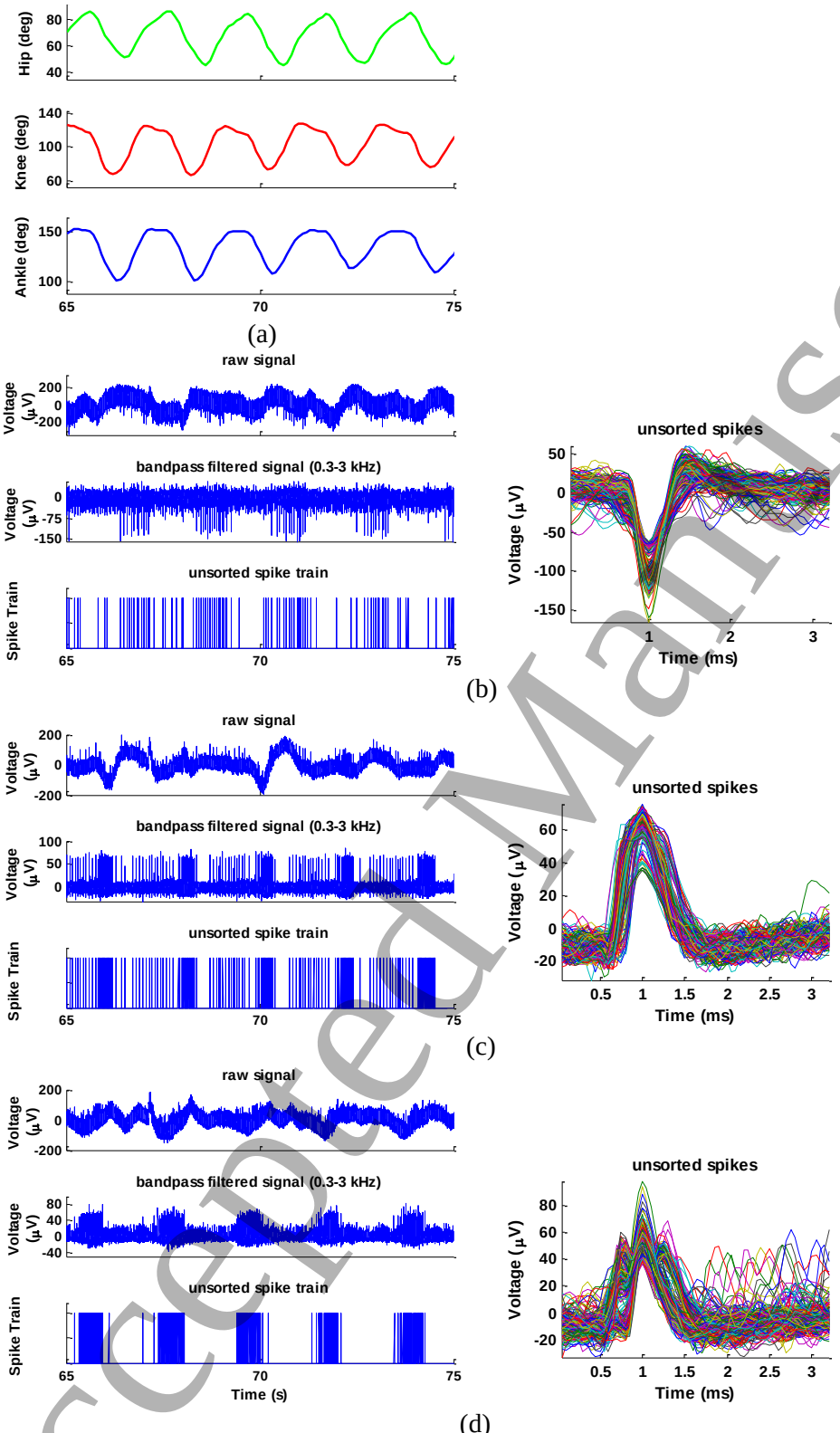

Figure 4. Typical measured joint angles and recorded neural signals from the dorsal horn neurons during passive movement (Cat 5 session 2): measured joint angles (a), raw and band-pass filtered (0.3-3 kHz) neural signals, unsorted spike trains, and spikes waveforms recorded from L4 (b), L5 (c), and L6 (d) vertebrae.

Accepted Manuscript

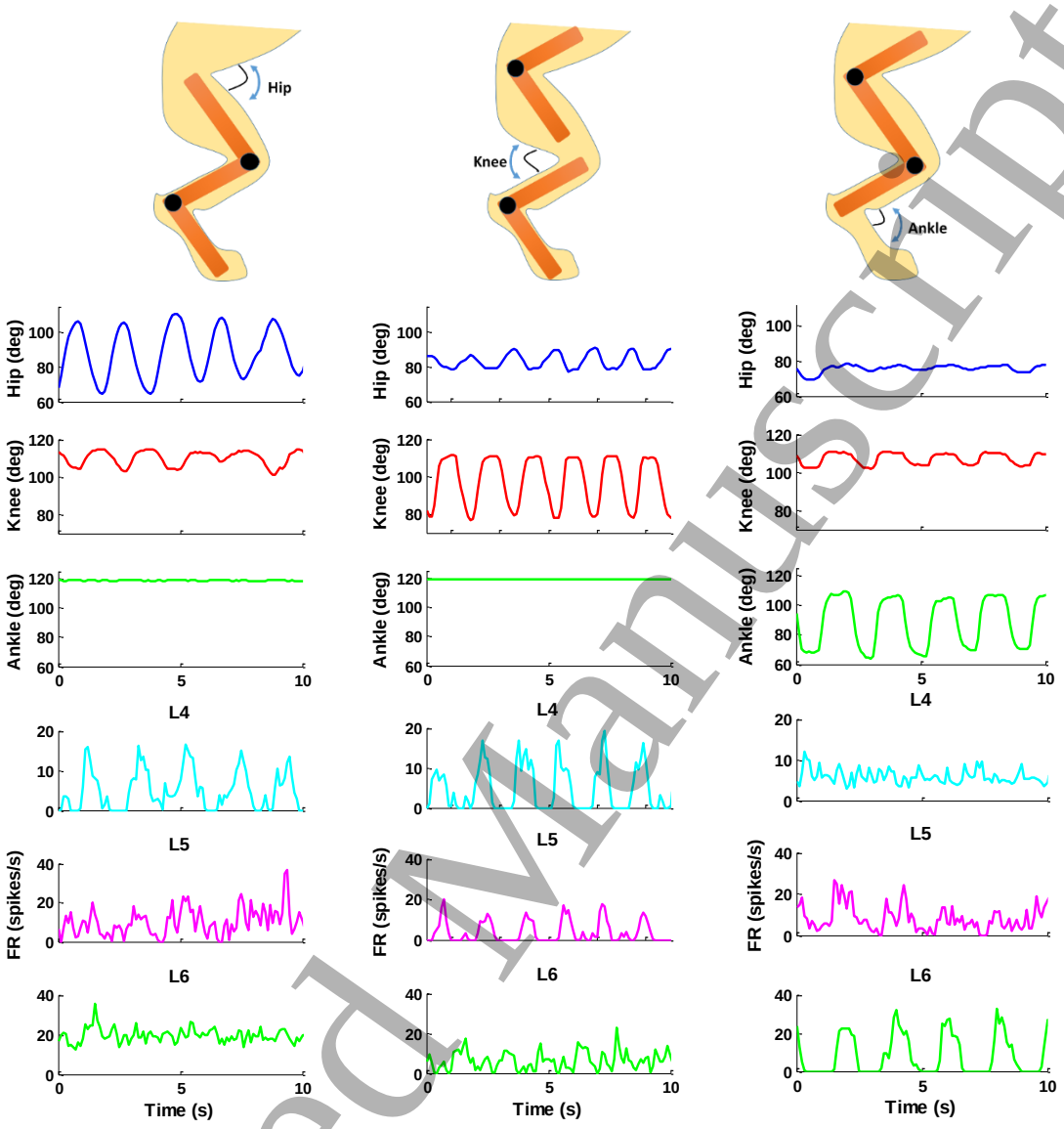

Figure 5. Firing rates of multi-unit activities recorded from L4, L5, and L6 vertebral segments during passive movement of the hip (a), knee (b), and ankle (c) joints (cat 6 session 1). During this experiment, only one joint was passively flexed or extended while other two joints were held fixed as much as possible.

Figure 6(a) shows the average of mutual information between the firing rate of the neural signal recorded from each segment and each joint angle trajectory, over 70 trials of experiment on three cats. The results of this analysis indicate that the neural activity recorded from each segment contains information about all joints, but the neural signal recorded from the L4 provides the highest information about the kinematics of the hip joint, the neural signal from the L5 about the knee joint, and the L6 about the ankle joint. Figures 6(b) and (c) show the average of decoding performance over 70 trials of experiment on three cats, using the recorded firing rates from the L4, L5, and L6 vertebral segments. It is observed that the best performance

Accepted Manuscript

for the hip joint was obtained using the signal recorded from the L4. For the knee movement, the decoding performance obtained using the signal recorded from the L5 was higher than that obtained using signal from either L4 or L6. For the ankle joint, the best decoding performance was obtained using the signal recorded from the L6.

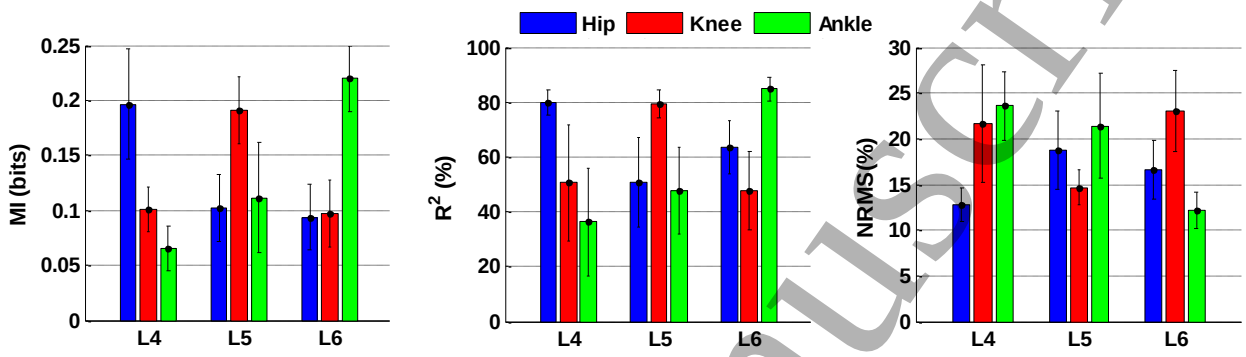

(a) (b) (c)

Figure 6. (a) Average mutual information between firing rates of the neural signals recorded from each vertebral segment (i.e., L4, L5, and L6) and joint angle trajectory of each joint. (b) Average decoding performance of each joint angle using the firing rates recorded from each vertebral segment. (c) Average NRMS decoding error of each joint angle using the firing rates recorded from each vertebral segment. Results are averaged over 70 trials of experiment on three cats for each joint. Error bar on each bar graph represents standard deviation over 70 trials.

5.2 Multi-joint decoding

Figure 7(a) shows typical recorded joint angles and corresponding continuous FRs during passive movement of the three joints for cat 3 (session 1). It is observed that the FR activity recorded from L4 vertebra closely matched with the hip angle trajectory. The FR increased with increasing the hip extension and decreased with decreasing the extension. The FR of the recorded neural signal from the L5 began to increase as the knee began to increase and reached the maximum with the full extension of the knee. As the knee begun to flex, the FR fell to zero. The peak of the FR of the signal recorded from the L6 corresponded to the full flexion of the ankle joint. Figure 7(b) shows another trial of experiment with different movement speeds for Cat 5 (session 2). The same phenomena were also observed.

Accepted Manuscript

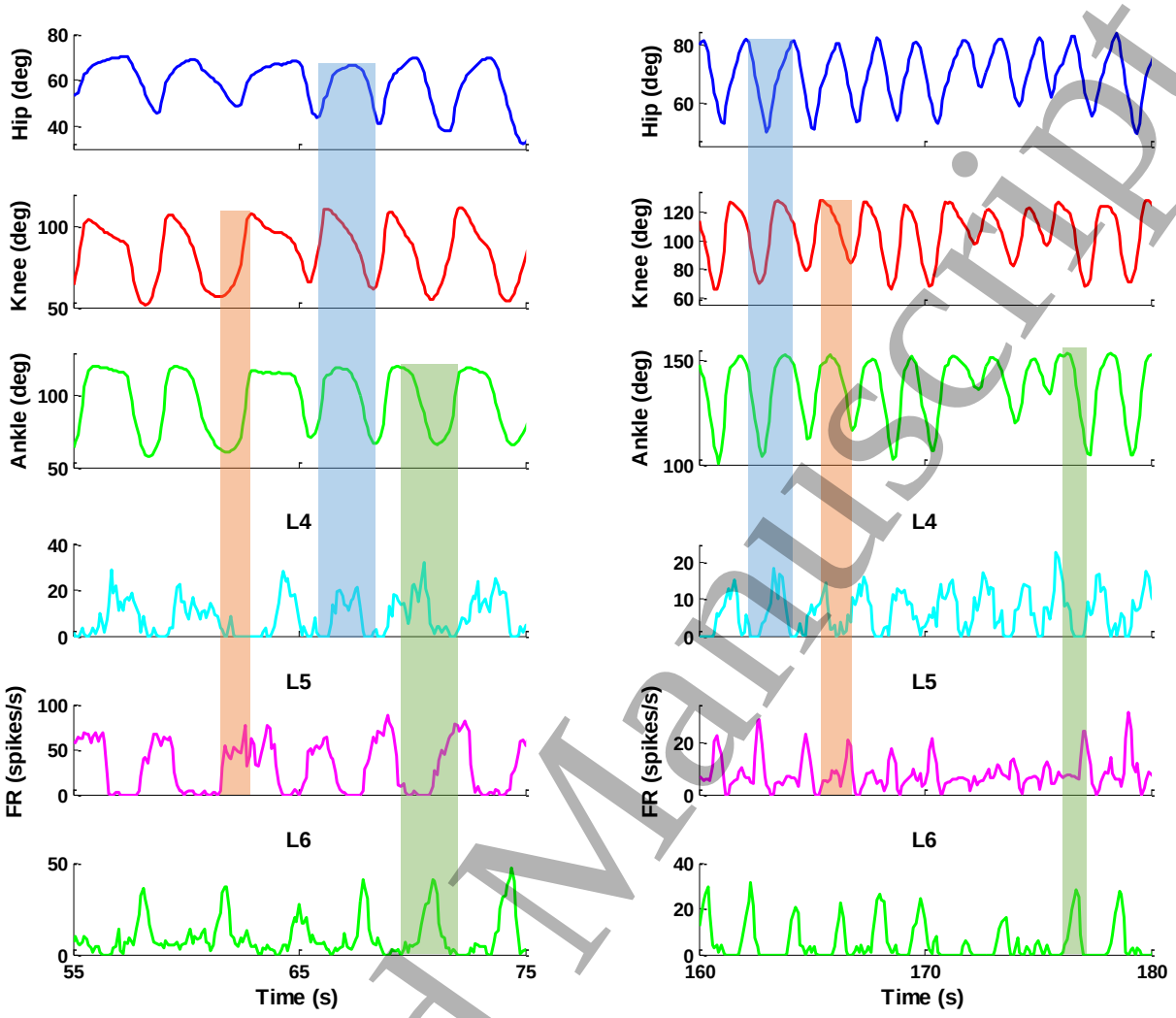

Figure 7. Example of recorded joint angles and continuous firing rate of neural activities recorded from L4, L5, and L6 for two cats: (a) cat 3 session 1, (b) cat 5 session 2.

Table 2 summarizes the results of the decoding hind limb kinematics using the proposed method with using single-segment and multi-segment recordings during multi-joint movement. It is observed that the L4 recording provided lower decoding error (9.5%) for the hip joint than that for the knee and ankle joints, the L5 recording provided lower decoding error (11.7%) for the knee joint than that for other joints, and the L6 recording for the ankle (10.6%). Nevertheless, the multi-segment recordings consist of the L4, L5, and L6 recordings achieve the best decoding performance. The decoding errors are 7.8%, 8.2%, and 8.4% for the hip, knee, and ankle joints, respectively. To evaluate the statistical significance, Wilcoxon signed rank test was performed on NRMS errors and R^2 values obtained using single-electrode and multi-electrode recordings. This analysis revealed that multi-segment decoding significantly outperformed single segment decoding for each joint angle ($p < 0.001$). The results show that the decoding performances obtained by

Accepted Manuscript

the L4, L5, and L6 vertebral segments are approximately equal for the knee joint angle. The errors are 11.4%, 11.7%, and 11.3% for L4, L5, and L6, respectively.

Table 2. Average of decoding performance over eight sessions of experiment on five cats using proposed probabilistic recurrent neural network for different joint angles.

Spinal vertebrae	Joint Angle	R^2 %	NRMS %
L4	Hip	80.1 ± 3.3	9.5 ± 1.2
	Knee	78.5 ± 3.9	11.4 ± 1.6
	Ankle	79.4 ± 3.7	11.0 ± 1.3
	Average	79.3 ± 4.2	10.6 ± 1.7
L5	Hip	68.0 ± 5.0	12.3 ± 1.9
	Knee	75.5 ± 3.3	11.7 ± 1.5
	Ankle	68.2 ± 4.7	13.6 ± 2.0
	Average	70.5 ± 5.1	12.5 ± 2.2
L6	Hip	74.5 ± 3.8	11.1 ± 1.4
	Knee	78.5 ± 4.1	11.3 ± 1.8
	Ankle	82.9 ± 3.2	10.6 ± 1.6
	Average	78.6 ± 4.3	11.0 ± 1.7
All (L4, L5, L6)	Hip	86.8 ± 2.2	7.8 ± 0.7
	Knee	87.6 ± 2.0	8.2 ± 0.9
	Ankle	89.0 ± 2.3	8.4 ± 1.0
	Average	87.8 ± 2.4	8.1 ± 1.0

Figure 8 shows the typical decoding the limb kinematics from the neural signals recorded from L4, L5, and L6 vertebrae using the proposed method for two cats. It is observed that accurate decoding of the joint angles was achieved. The NRMS errors obtained using the proposed method for cat 3 (session 1) are 5.8%, 6.6%, and 7.4 for the hip, knee, and ankle joints, respectively. The coefficients of determination obtained are 90.0%, 93.3%, and 94.4% for this trial of experiment. For cat 5 (session 2) NRMS errors are 6.2%, 6.9%, and 7.2% for the hip, knee, and ankle joints respectively. The coefficients of determination obtained are 93.4%, 91.9%, and 91.5% for this trial of experiment.

Accepted Manuscript

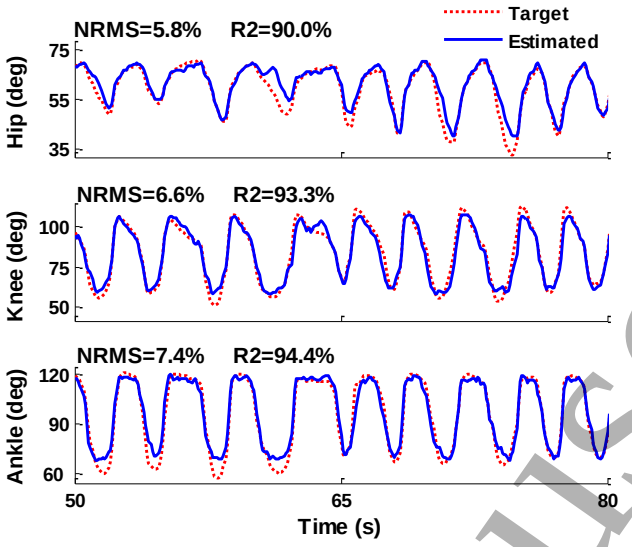

(a)

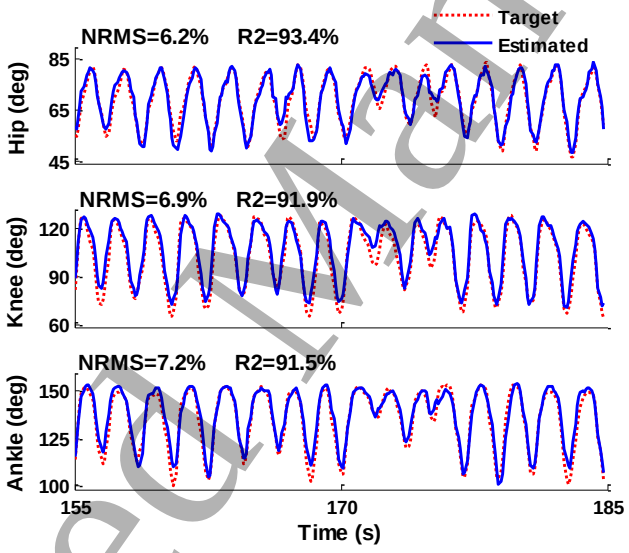

(b)

Figure 8. Examples of decoding hind limb kinematics using PRNN model with combined FRs recorded from L4, L5, and L6 vertebral segments for two cats: (a) cat 3 session 1, (b) cat 5 session 2.

Table 3 summarizes the performances obtained using the proposed PRNN, Kalman filter [43], and a conventional recurrent neural network which is based on the state-space model [31]. In this architecture, the output of the hidden layer is fed back to the input layer via a bank of unit-time delays. The hidden layer of the RNN used in this experiment consists of ten neurons. An average decoding error of 11.5%, 9.3%, and 8.1% was obtained using Kalman, RNN, and PRNN, respectively. The average coefficients of determination values obtained are 76.3%, 84.5%, and 87.8%, respectively. The results of the Wilcoxon signed rank statistical tests show that PRNN significantly outperformed Kalman filter ($p < 0.001$) and RNN ($p < 0.05$).

Accepted Manuscript

Table 3. Average of decoding performance using different methods with combined neural signals recorded from L4, L5, and L6. Results are averaged over eight sessions of experiment on five cats.

Method	Joint Angle	R^2 %	NRMS %
Kalman	Hip	73.7 ± 2.4	11.1 ± 1.1
	Knee	76.6 ± 2.4	11.7 ± 1.9
	Ankle	78.7 ± 1.8	11.9 ± 1.4
	Average	76.3 ± 2.2	11.5 ± 1.9
RNN	Hip	82.8 ± 3.8	8.9 ± 1.3
	Knee	84.8 ± 3.6	9.3 ± 1.4
	Ankle	86.1 ± 2.4	9.7 ± 1.0
	Average	84.5 ± 3.3	9.3 ± 1.5
PRNN	Hip	86.8 ± 2.2	7.8 ± 0.7
	Knee	87.6 ± 2.0	8.2 ± 0.9
	Ankle	89.0 ± 2.3	8.4 ± 1.0
	Average	87.8 ± 2.4	8.1 ± 1.0

6. Discussion and conclusion

In this study, a generative probabilistic model with an adaptive discriminative learning is proposed for decoding the limb kinematics from the extracellular recording of dorsal horn gray matter of the spinal cord during passive limb movement. The generative model is based on the joint distribution of the input and output variables and is learned in a discriminative manner. The model does not require any presumption about the joint distribution of the process. It was shown that the model can be represented by an RNN while its structure was determined by the model itself. The results show that the proposed method provides an accurate decoding the limb kinematics. The average decoding errors are 10.6%, 12.5%, and 11.0% using the neural signals recorded from the L4, L5, and L6 vertebral segments, respectively. The neural signals recoded from the L4 provide higher decoding accuracy than that from the L5. Compared to the previous work [28], an improvement of 1.4% in decoding error and 4.4% in R^2 was obtained using the proposed method with the neural signal recorded from the L6 vertebra.

The results indicated that the combined signals from multi-segment provided a robust decoding performance than single-segment recordings. Compared to single-segment recordings in [28], an improvement of 4.3% in NRMS error and 13.6 % in R^2 were achieved when the combined signals from the L4, L5, and L6 vertebrae were used for decoding.

Our results show that the hind limb kinematics information are distributed rostrocaudally through different segments of the spinal cord. The results show that the L4 provide more information about the hip joint, the L5 vertebra about the knee, and the L6 about the ankle joint. Our results show that the hip, knee, and ankle angles can be decoded using single-electrode recording from one vertebral segment (L4, L5, or

Accepted Manuscript

L6) with acceptable accuracy. This suggests that the hind limb kinematics information are distributed rostrocaudally through different segments of the spinal cord. The results obtained are consistent with the previous reports [46, 47]. It has been shown that the removal of the sensory inputs to the L3/4 spinal segments removes the information concerning the hip position whilst the L5-S1 deafferentation leaves those inputs intact but removes all of the load information [47]. In [46], it was shown that the L6 DRG responded mainly to extension and flexion of the hip and knee, whereas L7 DRG responded mainly to extension and flexion of the toe and ankle. It should be noted that the nerve fibers from L6 and L7 DRGs enter the L5 and L6 vertebral segments of the spinal cord, respectively.

The proposed decoding strategy in this paper has provided very promising results for developing a chronically implanted prosthetic device. Nevertheless, there are still challenges including the fabrication and implantation of the intraspinal microwires. Additionally, implanting microwires into the body always carries the risk of infection and migration. However, recent progress in microwire fabrication [48] can be applied to reduce the risk. Moreover, our results show that all joint kinematic information can be decoded using only one implanted electrode while the intracortical and ECoG recordings require a large number of electrodes to be implanted into the brain [8-12].

The discretizing process of the proposed generative model is limited to one dimensional dynamics. The extension of the current study to higher dimension dynamics will be considered as the object of the future study.

Acknowledgments

This work was supported by the Iran Neural Technology Research Centre, Tehran, Iran under Grant 48.M.111194. There are no conflicts of interest for the authors of this study.

Appendix A

Based on the conditional probability definition, (2) can be written as

$$\hat{y}_n = \int y_n p(y_n|\mathbf{x}_n, \mathbf{X}_{n-1})\, dy_n = \int y_n \frac{p(y_n,\mathbf{x}_n,\mathbf{X}_{n-1})}{p(\mathbf{x}_n,\mathbf{X}_{n-1})} dy_n \quad \text{(A-1)}$$

$$= \int y_n \frac{p(\mathbf{x}_n|y_n,\mathbf{X}_{n-1})p(y_n,\mathbf{X}_{n-1})}{p(\mathbf{x}_n|\mathbf{X}_{n-1})p(\mathbf{X}_{n-1})}\, dy_n \quad \text{(A-2)}$$

$$= \frac{\int y_n\, p(\mathbf{x}_n|y_n,\mathbf{X}_{n-1})p(y_n|\mathbf{X}_{n-1})p(\mathbf{X}_{n-1})dy_n}{p(\mathbf{x}_n|\mathbf{X}_{n-1})p(\mathbf{X}_{n-1})} \quad \text{(A-3)}$$

Based on the Chapman-Kolmogorov equation [49] ($p(\mathbf{x}_n|\mathbf{x}_{n-1}) = \int p(\mathbf{x}_n|y_n)p(y_n|\mathbf{x}_{n-1})\, dy_n$), the denominator of (A-3) can be rewritten as

$$\hat{y}_n = \frac{\int y_n\, p(\mathbf{x}_n|y_n,\mathbf{X}_{n-1})p(y_n|\mathbf{X}_{n-1})\, dy_n}{\int p(\mathbf{x}_n|y_n)p(y_n|\mathbf{X}_{n-1})dy_n} \quad \text{(A-4)}$$

Accepted Manuscript

It is assumed that the current measurement $\mathbf{x}_n$ given the current state y_n is conditionally independent of the measurement and state histories:

$$p(\mathbf{x}_n|y_n, \mathbf{X}_{n-1}) = p(\mathbf{x}_n|y_n) \quad \text{(A-5)}$$

Then, (A-4) can be written as

$$\hat{y}_n = \frac{\int y_n \, p(\mathbf{x}_n|y_n) p(y_n|\mathbf{X}_{n-1}) \, dy_n}{\int p(\mathbf{x}_n|y_n) p(y_n|\mathbf{X}_{n-1}) dy_n} \quad \text{(A-6)}$$

Applying the Chapman-Kolmogorov equation ($p(y_n|\mathbf{X}_{n-1}) = \int p(y_n|y_{n-1}) p(y_{n-1}|\mathbf{X}_{n-1}) \; dy_{n-1}$) to (A-6), we can write

$$\hat{y}_n = \frac{\int y_n \, p(\mathbf{x}_n|y_n) \int p(y_n|y_{n-1}) p(y_{n-1}|\mathbf{X}_{n-1}) \, dy_{n-1} dy_n}{\int p(\mathbf{x}_n|y_n) \int p(y_n|y_{n-1}) p(y_{n-1}|\mathbf{X}_{n-1}) \, dy_{n-1} \; dy_n} \quad \text{(A-7)}$$

References

[1] Haugland M K and Sinkjær T 1995 Cutaneous whole nerve recordings used for correction of footdrop in hemiplegic man *IEEE Trans. Rehabil. Eng.* **3** 307–17

[2] Haugland M, Lickel A, Haase J and Sinkjaer T 1999 Control of FES thumb force using slip information obtained from the cutaneous electroneurogram in quadriplegic man *IEEE Trans. Rehabil. Eng.* **7** 215–27

[3] Strange K D and Hoffer J A 1999 Restoration of use of paralyzed limb muscles using sensory nerve signals for state control of FES-assisted walking *IEEE Trans. Rehabil. Eng.* **7** 289–300

[4] Riso R R, Mosallaie F K, Jensen W and Sinkjaer T 2000 Nerve cuff recordings of muscle afferent activity from tibial and peroneal nerves in rabbit during passive ankle motion *IEEE Trans. Rehabil. Eng.* **8** 244–58

[5] Micera S, Jensen W, Sepulveda F, Riso R R and Sinkjær T 2001 Neuro-fuzzy extraction of angular information from muscle afferents for ankle control during standing in paraplegic subjects: An animal model *IEEE Trans. Biomed. Eng.* **48** 787–94

[6] Hansen M, Haugland M K and Sinkjær T 2004 Evaluating robustness of gait event detection based on machine learning and natural sensors. *IEEE Trans Neural Syst Rehabil Eng* **12** 81–8

[7] Bruns T M, Wagenaar J B, Bauman M J, Gaunt R A and Weber D J 2013 Real-time control of hind limb functional electrical stimulation using feedback from dorsal root ganglia recordings *J. Neural Eng.* **10** 026020

[8] Fitzsimmons N A, Lebedev M A, Peikon I D and Nicolelis M A L 2009 Extracting kinematic parameters for monkey bipedal walking from cortical neuronal ensemble activity *Front. Integr. Neurosci.* **3** 1–19

[9] Rigosa J, Panarese A, Dominici N, Friedli L, Van Den Brand R, Carpaneto J, Digiovanna J, Courtine

Accepted Manuscript

G and Micera S 2015 Decoding bipedal locomotion from the rat sensorimotor cortex *J. Neural Eng.* **12** 56014

[10] Chao Z C, Nagasaka Y and Fujii N 2010 Long-term asynchronous decoding of arm motion using electrocorticographic signals in monkeys *Front. Neuroeng.* **3**

[11] Flint R D, Rosenow J M, Tate M C and Slutzky M W Continuous decoding of human grasp kinematics using epidural and subdural signals *J. Neural Eng.* **14** 016005

[12] Farrokhi B and Erfanian A A piecewise probabilistic regression model to decode hand movement trajectories from epidural and subdural ECoG signals *J. Neural Eng.* **15** 036020

[13] Holinski B J, Everaert D G, Mushahwar V K and Stein R B 2013 Real-time control of walking using recordings from dorsal root ganglia *J. Neural Eng.* **10** 056008

[14] Stein R B, Weber D J, Aoyagi Y, Prochazka A, Wagenaar J B M, Shoham S and Normann R A 2004 Coding of position by simultaneously recorded sensory neurones in the cat dorsal root ganglion *J. Physiol.* **560** 883–96

[15] Weber D J, Stein R B, Everaert D G and Prochazka A 2006 Decoding sensory feedback from firing rates of afferent ensembles recorded in cat dorsal root ganglia in normal locomotion *IEEE Trans. Neural Syst. Rehabil. Eng.* **14** 240–3

[16] Weber D J, Stein R B, Everaert D G and Prochazka A 2007 Limb-state feedback from ensembles of simultaneously recorded dorsal root ganglion neurons *J. Neural Eng.* **4** S168-80

[17] Wagenaar J B, Ventura V and Weber D J 2011 State-space decoding of primary afferent neuron firing rates *J. Neural Eng.* **8** 016002

[18] Rigosa J, Weber D J, Prochazka A, Stein R B and Micera S 2011 Neuro-fuzzy decoding of sensory information from ensembles of simultaneously recorded dorsal root ganglion neurons for functional electrical stimulation applications *J. Neural Eng.* **8** 046019

[19] Han S, Chu J U, Kim H, Park J W and Youn I 2017 Multiunit activity-based real-time limb-state estimation from dorsal root ganglion recordings *Sci. Rep.* **7** 44197

[20] Han S, Chu J U, Kim H, Choi K, Park J W and Youn I 2016 An unsorted spike-based pattern recognition method for real-time continuous sensory event detection from dorsal root ganglion recording *IEEE Trans. Biomed. Eng.* **63** 1310–20

[21] Borisoff J F, Mcphail L T, Saunders J T W, Birch G E and Ramer M S 2006 Detection and classification of sensory information from acute spinal cord recordings *IEEE Trans. Biomed. Eng.* **53** 1715–19

[22] Bosco G and Poppele R E 2000 Reference frames for spinal proprioception: kinematics based or kinetics based? *J. Neurophysiol.* **83** 2946–55

[23] Bosco G and Poppele R E 2001 Proprioception from a spinocerebellar perspective. *Physiol. Rev.* **81**

Accepted Manuscript

539–68

[24] Bosco G 2003 Modulation of dorsal spinocerebellar responses to limb movement. II. effect of sensory input *J. Neurophysiol.* **90** 3372–83

[25] Bosco G, Eian J and Poppele R E 2006 Phase-specific sensory representations in spinocerebellar activity during stepping: Evidence for a hybrid kinematic/kinetic framework *Exp. Brain Res.* **175** 83–96

[26] Kandel E R, Schwartz J H and Jessell T M 2000 *Principles of Neural Science* (New York: McGraw-hill)

[27] Im C, Park H Y, Koh C S, Ryu S B, Seo I S, Kim Y J, Kim K H and Shin H C 2016 Decoding intravesical pressure from local field potentials in rat lumbosacral spinal cord *J. Neural Eng.* **13** 056005

[28] Yeganegi H, Fathi Y and Erfanian A 2018 Decoding hind limb kinematics from neuronal activity of the dorsal horn neurons using multiple level learning algorithm *Sci. Rep.* **8** 577

[29] Song K Il, Chu J U, Park S E, Hwang D and Youn I 2017 Ankle-angle estimation from blind source separated afferent activity in the sciatic nerve for closed-loop functional neuromuscular stimulation system *IEEE Trans. Biomed. Eng.* **64** 834–43

[30] Wu W, Black M J, Mumford D, Gao Y, Bienenstock E and Donoghue J P 2004 Modeling and decoding motor cortical activity using a switching Kalman filter *IEEE Trans. Biomed. Eng.* **51** 933–42

[31] Haykin S 2009 *Neural Networks and Learning Machines* (Upper Saddle River: Pearson Education)

[32] Ng A Y and Jordan M I 2002 On discriminative vs. generative classifiers: A comparison of logistic regression and naive Bayes *Adv. Neural Inf. Process. Syst.* **14** 841–8

[33] Bishop C M and Lasserre J 2007 Generative or discriminative ? getting the best of both worlds *Bayesian Stat.* **8** 3–24

[34] Posner I and Ondr P 2016 Deep tracking: seeing beyond seeing using recurrent neural networks arXiv:1602.00991

[35] Haarnoja T, Ajay A, Levine S and Abbeel P 2016 Backprop KF : learning discriminative deterministic state estimators *30th conf. on Neural Information Processing Systems (Barcelona, Spain).*

[36] Mense S and Craig A D 1988 Spinal and supraspinal terminations of primary afferent fibers from the gastrocnemius-soleus muscle in the cat *Neuroscience* **26** 1023–35

[37] Brown P B, Gladfelter W E, Culberson J C, Covalt-Dunning D, Sonty R V., Pubols L M and Millecchia R J 1991 Somatotopic organization of single primary afferent axon projections to cat spinal cord dorsal horn *J. Neurosci.* **11** 298–309

Accepted Manuscript

[38] Pe A, Escolano F and Juan M S 2009 Learning Gaussian mixture models with entropy based criteria *IEEE Trans. Neural Networks* **20** 1756–71

[39] De Jesus O and Hagan M T 2007 Backpropagation algorithms for a broad class of dynamic networks *IEEE Trans. Neural Networks* **18** 14–27

[40] Hagan M T, Demuth H B, Beale M and Jesús O De 2014 *Neural Network Design* (Stillwater: Martin Hagan)

[41] Brockwell A E, Rojas A L and Kass R E 2004 Recursive Bayesian decoding of motor cortical signals by particle filtering *J. Neurophysiol.* **91** 1899–907

[42] Kemere C, Shenoy K V and Meng T H 2004 Model-based neural decoding of reaching movements : a maximum likelihood approach *IEEE Trans. Biomed. Eng.* **51** 925–32

[43] Wu W, Gao Y, Bienenstock E, Donoghue Ü J P and Black Ü M J 2006 Bayesian population decoding of motor cortical activity using a Kalman filter *Neural Comput.* **18** 80–118

[44] Langlet C, Leblond H and Rossignol S 2005 Mid-lumbar segments are needed for the expression of locomotion in chronic spinal cats *J. Neurophysiol.* **93** 2474–88

[45] Darbellay G A and Vajda I 1999 Estimation of the information by an adaptive partitioning of the observation space *IEEE Trans. Inf. THEORY* **45** 1315–21

[46] Aoyagi Y, Stein R B, Branner A, Pearson K G and Normann R A 2003 Capabilities of a penetrating microelectrode array for recording single units in dorsal root ganglia of the cat *J. Neurosci. Methods* **128** 9–20

[47] Norton J A and Mushahwar V K 2010 Afferent inputs to mid- and lower-lumbar spinal segments are necessary for stepping in spinal cats *Ann. N. Y. Acad. Sci.* **1198** 10–20

[48] Bamford J A, Lebel R M, Parseyan K and Mushahwar V K 2017 The fabrication, implantation, and stability of intraspinal microwire arrays in the spinal cord of cat and rat *IEEE Trans. Neural Syst. Rehabil. Eng.* **25** 287–96

[49] Särkkä S 2013 *Bayesian Filtering and Smoothing* (Cambridge: Cambridge University Press)1–232

Accepted Manuscript